(13) An authentic sample of the acylurea of *p*-toluic acid was prepared as shown below

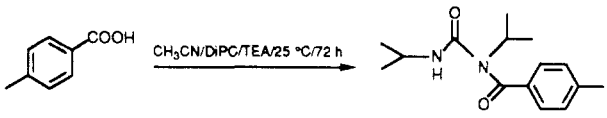

^{1}H NMR ($CDCl_3$) δ 0.99 (d, 6 H), 1.42 (d, 6 H), 2.39 (s, 3 H), 3.84 (m, 1 H), 4.41 (m, 1 H), 6.80 (br s, 1 H), 7.21 (d, 2 H), 7.41 (d, 2 H); ^{13}C NMR ($CDCl_3$) δ 20.87 (q), 21.40 (q), 22.26 (q), 42.61 (d), 50.35 (d), 126.49 (d), 129.17 (d), 134.2 (s), 141.01 (s), 154.25 (s), 172.63 (s). MS EI (70 eV), *m/z* (relative intensity) 262 (9%, M^+), 176 (14), 162 (20), 119 (100), 91 (28), 58 (20).

(14) DeTar, D. F.; Silverstein, R. *J. Am. Chem. Soc.* **1966**, *88*, 1013.
(15) Moore, J. S.; Stupp, S. I. Low Symmetry Macromolecules. I. Synthesis. Submitted for publication.
(16) Bhama, S.; Stupp, S. I., unpublished results from this laboratory.

(17) Deuterium labeling was achieved as shown below

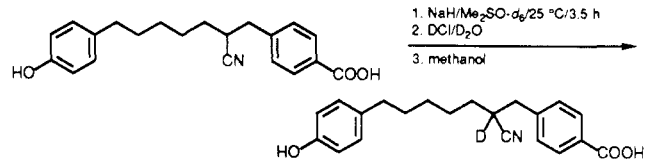

Deuterium coupling in the ^{13}C NMR specified the isotopic site at the nitrile α-position. The percent deuterium incorporated was determined to be 94.3% by field ionization mass spectrometry and NMR measurements. ^{1}H NMR δ (Me_2SO-d_6) 1.30 (M, 2 H), 1.53 (m, 6 H), 2.44 (t, 2 H), 2.93 (ABq, 2 H), 6.65 (d, 2 H), 6.95 (d, 2 H), 7.41 (d, 2 H), 7.90 (d, 2 H), 9.10 (s, 1 H), 12.91 (br s, 1 H). ^{13}C NMR (acetone-d_6) δ 27.45 (t), 29.12 (t), 32.17 (t), 32.30 (t), 33.49 (t, C(D)CN, J(CD) = 20.6 Hz), 35.31 (t), 38.42 (t), 115.75 (d), 122.11 (s), 129.95 (d), 130.07 (d), 130.59 (d), 133.90 (s), 144.08 (s), 156.05 (s), 167.50 (s).

Thermal Aging of Tetraalkyl Ammonium Doped Polyacetylenes

Francis Ignatious and Claude Mathis*

Institut Charles Sadron (CRM-EAHP) (CNRS-ULP), 6 rue Boussingault, 67083 Strasbourg Cedex, France. *Received January 30, 1989; Revised Manuscript Received May 4, 1989*

ABSTRACT: The stability of tetraalkyl ammonium doped polyacetylenes was examined under accelerated conditions by monitoring the evolution of their intrinsic properties by utilizing electrical conductivity, DSC, and ESR measurements. A first-order rate equation was deduced from the electrical measurements, which leads to an apparent activation energy of about 28 kcal/mol for the counterions studied. A simple mechanism for this inherent instability, which stems from the protonation of the doped sites by the tetraalkyl ammonium ions, was suggested and was verified by elemental analysis and IR spectral studies of the degraded films and also by the gas chromotographic analysis of the degradation products. An ion-exchange method was devised to surpass the 7% doping level attainable by the direct reduction with the R_4N^+ ion doping agents. The behavior of reduced β-carotene, considered to be the soluble analogue of the insoluble PA, toward its R_4N^+ counterion was investigated, and a similar proton abstraction mechanism was put forward to explain its reactivity. In all cases, the order of reactivities of the carbanions were rationalized on the basis of their redox potentials.

Introduction

Developments in the field of conducting polymers have been retarded due to their extreme sensitivity to ambient atmospheric conditions. Both the parent conjugated system and its doped form (oxidized or reduced) are subject to losing their inherent interesting properties. The deterioration of the properties of the doped form may be attributed to extrinsic or intrinsic factors. The extrinsic instability of the doped polyacetylene (PA), taken as the prototype of conducting polymers, arises from the reactivity of the polycarbanion or polycarbenium ion toward moisture or other reactive species. On the other hand, the intrinsic stability of the system is controlled by the reaction between the dopant ion and the polymer backbone and hence is dopant dependent. Investigations on the p-doped PA have revealed that the iodine-oxidized films are relatively less stable than that obtained from AsF_5.[1] Similar studies by Pochan et al.[2] and by Druy et al.[3] have demonstrated that iodine- and perchlorate-doped samples lose their conductivity quite rapidly under vacuum, due to the reaction of the polymer backbone with the counterion. Yang et al.[4] also observed the instability of these doped polymers and pointed out that the reaction of PA with perchlorate counterions can be explosive.

In contrast, alkali-metal-doped PA exhibits intrinsic stability and leads to a dopant cation-dependent conductivity enhancement during thermal annealing.[5] While realizing the electrochemical insertion of R_4N^+ ions into PA, MacDiarmid et al.[6] have remarked on the degradation of the properties of the PA electrode. We have accomplished a similar insertion of organic cations by a purely chemical method, by developing a complex carbanionic dopant system that functions by a guest cation insertion mechanism.[7] The classical insertion technique becomes irrelevant in this case due to the extreme reactivity of the carbanions with the R_4N^+ counterions. This reactivity is governed by the basicity of the carbanions, which can be correlated with their redox potentials. It then becomes interesting to examine how a polycarbanion, existing as a highly delocalized system but confined to the solid state, interacts with its countercation. We have undertaken a detailed study of the kinetics and mechanism of the degradation of the R_4N^+-doped PA. In order to better define the reactivity of a reduced polyenic sys-

0024-9297/90/2223-0070$02.50/0

tem, present in a homogenous medium, toward NR_4^+ ions, we have carried out a parallel study on β-carotene, a commercially available product possessing 11 conjugated double bonds.

Experimental Section

All experiments were performed in suitably designed glass apparatus sealed under vacuum and by making use of break-seals whereever necessary, such that all steps from the doping reaction up to the measurements were done in situ. A modified Shirakawa technique[8] was utilized in the synthesis of the PA films, yielding the cis isomer for the synthesis performed at −78 °C. Thermal isomerizations were carried out by heating the films at 180 °C for about 15 min under vacuum.

The films used in this study were doped to Y values of 6–7% by exercising thermodynamic control of the doping level ($Y = R_4N^+/CH$) employing the complex dopant system (barium benzophenone dianion/THF/R_4NBr) described earlier.[7]

For the electrical measurements, pressed electrical contacts were connected to the external leads through vacuum-tight outlets integrated into a glass apparatus as described earlier.[9] The electrical contacts were attached to the films in a drybox (with less than 0.2 ppm oxygen and 1 ppm water). The glass apparatus was subsequently evacuated on a high-vacuum line and sealed. The films were immersed in the dopant solution by crushing the break-seal that separates the dopant solution from the rest of the apparatus. When the conductivities were stabilized, the films were washed thoroughly by the internal distillation of THF. The doped films, kept at 25 °C, were dried by cryogenic pumping, cooling the glass bulb containing the dopant solution to −78 °C. This glass bulb was then sealed off. The glass apparatus containing the doped films was immersed in a constant-temperature oil bath, and the resistances were monitored by a Keithly 195 multimeter interfaced with a computer.

The R_4N^+ ion doped PA samples for the DSC analysis were prepared, under vacuum, by immersing the PA samples for 48 h in the dopant solution, followed by washing and drying. The glass bulb containing the doped films was sealed and opened in an ultrapure argon-filled drybox. Weighed pieces of the doped films were loaded in the drybox into air-tight stainless steel capsules. The DSC measurements were performed on a Perkin Elmer DSC-2 calorimeter.

The ESR studies were carried out in a sealed glass apparatus provided with an ESR tube such that the films are doped in situ under high vacuum. After the films were doped for about 48 h, they were washed and dried by cryogenic pumping. The dopant solution was then sealed off. The tubes containing the films were inserted in the magnetic cavity of a Brüker ESP 300 ESR spectrometer. The temperature of the cavity was regulated by a flux of preheated argon gas.

Synthesis of β-Carotene Dianion and Radical Anion. The commercial β-carotene was purified and carefully handled as previously described with necessary precautions to avoid any trace of proton donors.[10] The β-carotene dianion was synthesized in a glass apparatus provided with a glass filter and optical cell, which was flamed and sealed under vacuum, by reacting a THF solution of β-carotene over a sodium mirror. The resulting solution was filtered through a coarse frit into the quartz cell. The formation of the dianion was monitored by observing the appearance of the characteristic band at 790 nm. A few minutes of contact was sufficient for the complete conversion of β-carotene to its dianion. The dianionic solution thus formed was collected in the compartment containing the optical cell, and the rest of the glass apparatus was sealed off along with the glass filter. The β-carotene radical anion can be generated from the dianion by adding β-carotene until a new band at 830 nm appears and grows to maximum intensity at the expense of the band at 790 nm. This maximum is reached when one β-carotene per dianion is added. The ion exchanges to obtain the R_4N^+ salts of these anions were carried out by adding equivalent amounts of pure, dry R_4NBr.

Results and Discussion

(A) Stability of R_4N^+-Inserted PA. (1) Electrical Measurements. Measurement of electrical resistance provides an excellent means of monitoring the stability of the doped films as a function of time and temperature as it is very sensitive to the perturbation of the doped state. All the reported studies pertaining to the stability of the conducting polymers were followed by the variation of their electrical resistance. We have adopted a similar technique to look into the kinetics of the degradation of the R_4N^+ doped samples. Three different typical countercations, viz., Bu_4N^+, Oct_4N^+, and $Dodec_4N^+$ (Bu = butyl, Oct = octyl, and Dodec = dodecyl), were investigated in this work so as to assess the influence of the size of the cation on the stability of the doped product and to ascertain to what extent the steric hindrance imposed by the bulky cation can affect the reaction kinetics. Figure 1 depicts the variation of the resistance when a cis or trans doped film is heated progressively up to 100 °C (at each temperature the doped film was left for 30 min in order to attain equilibrium) and thereafter maintained at 100 °C for a few hours. Up to around 100 °C, we observe the expected decrease of the resistance due to the thermal activation as seen in the case of the other doped conducting polymers whereas, for longer times at 100 °C, the resistance exhibits an irreversible augmentation of several orders of magnitude. This irreversible increase of the resistance stems from the degradation of the doped films. In order to evaluate the kinetics of the degradation reaction, the samples were studied under four different isothermal conditions, viz., at 94, 110, 127, and 144 °C. The data are analyzed in light of a first-order kinetic equation

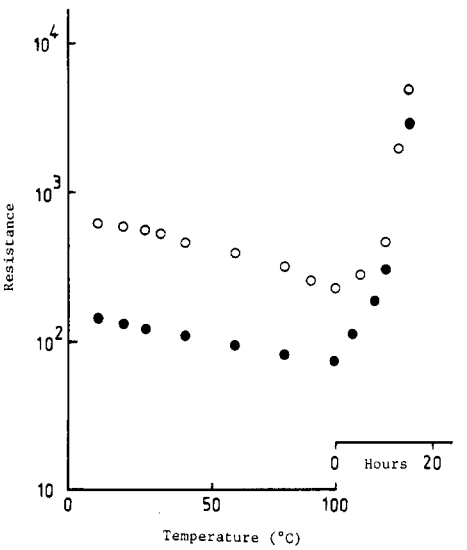

Figure 1. Variation of the resistances of Bu_4N^+-doped *cis*-PA (●) and *trans*-PA (○) films, with temperature up to 100 °C and thereafter as a function of time.

$$\ln R_t/R_0 = kt$$

where R_t represents the resistance of the sample at time t for a given fixed temperature and R_0 the one at time zero for the same temperature. Figure 2 shows the first-order plot of the degradation at 94 °C; from its slope the apparent rate constant is calculated. At higher temperatures the curve exhibits a linear first-order behavior for short times but deviates and tends to slow down at high decomposition levels. In such cases the initial slopes were utilized to calculate the rate constants.

From the calculated rate constants (Table I), it seems that the rate of degradation is sensitive to the size of the dopant cation, decreasing in the order $Dodec_4N^+ > Oct_4N^+ > Bu_4N^+$. Such a conclusion may be mislead-

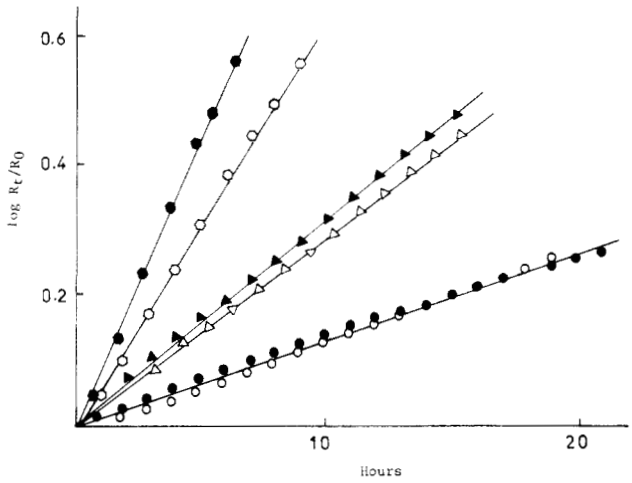

Figure 2. First-order kinetic plots for the degradation of doped-PA samples at 94 °C: ●, ▲, and ● represent Bu_4N^+-, Oct_4N^+-, and $Dodec_4N^+$-doped *cis*-PA samples and ○, △, and ○ their respective trans doped samples.

ing, as can be understood from the following considerations. We have earlier demonstrated that the room-temperature conductivities of the PA doped to the same level with R_4N^+ decrease as a function of their size.[9] The room-temperature conductivities of the Bu_4N^+- and $Dodec_4N^+$-doped samples are 1 and 10^{-2} S/cm, respectively. This effect has been explained by an increase of the interchain distance with the size of the cation, the electron hopping from chain to chain becoming more difficult. Thus, elimination of the same amount of conductive paths may lead to a greater diminution of the conductivity for PA inserted with larger cations. This could explain the apparent increase of rate constant of the degradation as the cation size increases.

The activation energies (E_A) are estimated from the Arrhenius plot (Figure 3). The values vary between 24 and 29 kcal/mol for the three cations studied, irrespective of the isomer involved (Table II). For a comparison, the activation energy values available in the literature for the decomposition of other doped conducting polymers are also included in Table II. Despite the fact that the mechanisms responsible for the degradation of the conducting polymers invoke in all cases the participation of a carbocation or a carbanion, the reported activation energies are scattered.

(2) DSC Measurements. The DSC experiments were performed in air-tight stainless steel capsules sealed under a dry argon atmosphere. Ito et al.[15] have previously reported that pristine PA does not thermally decompose in nitrogen until above 300 °C. The DSC analysis of our samples extended from 50 to 300 °C at a heating rate of 5°/min. Figure 4a shows a DSC thermogram of a Bu_4N^+-doped sample, which reveals an exothermic peak ranging from 120 to 190 °C, followed by an endotherm at 210 °C and a complete degradation of the sample at around 300 °C. A second sample was annealed up to 200 °C and cooled and scanned (Figure 4b). It does not exhibit the above-mentioned decomposition exotherm, but the endotherm persists. Figure 4c represents the DSC thermogram for Bu_4NBr at the same heating rate. It has two main endothermic peaks; the former at 100 °C corresponds to sublimation and the latter at 200 °C to pyrolysis of Bu_4NBr. These observations suggest that the DSC exotherm results exclusively from the reaction between the reduced PA and the Bu_4N^+ ion and not from the simple pyrolysis of the Bu_4N^+ ion, as may be argued. The endotherm could be assigned to the vaporization of the tertiary amine formed durig the decomposition. On the DSC thermograms obtained for the $Dodec_4N^+$ ion inserted cis and trans samples, only a single deactivation exotherm is observed. The peaks corresponding to the vaporization of the byproducts are absent as can be anticipated from their high boiling points. The characteristics of the thermograms are summarized in Table III. The DSC exotherms of the $Hept_4N^+$- and Hex_4N^+-doped samples (Hept = heptyl and Hex = hexyl) are complicated due to the superimposition of endotherms arising from the vaporization of their decomposition byproducts.

The DSC curves have been subjected to more detailed analysis to deduce the activation energy for the decomposition process, from the initial part of the DSC exotherm according to the method put forward by Rogers et al.[16] A plot of log d versus $1/T$ gives a straight line whose slope corresponds to $E_A/2.303R$. Here d is the distance of the peak from its base at the temperature T, and it is proportional to the heat envolved and the rate constant for the thermal decomposition at this temperature. E_A is the activation energy for the process. The frequency factor A is given by the expression

$$A = \frac{\varphi E e^{E/RT_{max}}}{RT_{max}^2}$$

where φ is the linear heating rate and T_{max} is the temperature at the maximum of the DSC exotherm. Figure 5 shows the Arrhenius plots for the Bu_4N^+ and $Dodec_4N^+$ complexes of *cis*-PA. The activation energies calculated for the three samples according to this method are also included in Table III. A comparison of the activation energies furnished by the conductivity and DSC techniques reveals that the former is systematically higher than the latter. This might be due to the difference in the experimental techniques and the inherent approximations made use of in arriving at the activation energy.

(3) ESR Measurements. ESR has been widely used in the investigations on PA as it presents a well-defined single-band spectrum that is sensitive to the slightest modification of the chemical environment of the system. The ESR spectral studies were performed in situ. The ESR peak-to-peak line widths and intensities were monitored as a function of the temperature ranging from 300 to 410 K, the sample being allowed to equilibrate for about 15 min at each temperature. The variations of the line widths and intensities are plotted as a function of temperature for the Bu_4N^+-doped *cis*-PA (Figure 6). The doped trans isomer also exhibits a similar behavior. Up to 370–380 K, the line widths are found to increase linearly with temperature, as was observed in the case of alkali-metal-doped PA.[17] As the temperature reaches about 100 °C, the line width deviates from the linear relationship and manifests an irreversible steep augmentation. This increase can be attributed to reduced spin mobility deriving its origin from the degradation of the doped sample. The variation of the intensity of the ESR band also reveals similar behavior. The intensity remains almost unaffected up to 100 °C, beyond which a sharp decrease is displayed. Such a decrease in intensity is probably due to the reduction in spin density arising from the destruction of the doped sites, as discussed in the next section.

(B) Mechanism of the Degradation Reaction. All the results discussed above point to an intrinsic instability of the system resulting from the reaction between the polycarbanion and the dopant cation. Analogous to the well-established mechanism prevailing in the interaction between the carbanions and R_4N^+ ions in

Table I
First-Order Rate Constants (s^{-1}) Calculated from Accelerated Aging under Isothermal Conditions of R_4N^+ Ion Doped PA (Y = 6–7%)

	Bu_4N^+		Oct_4N^+		$Dodec_4N^+$	
temp, °C	cis	trans	cis	trans	cis	trans
94	8.2×10^{-6}	9.1×10^{-6}	1.9×10^{-5}	2.3×10^{-5}	4.3×10^{-5}	5.8×10^{-5}
110	5.2×10^{-5}	2.0×10^{-5}			2.1×10^{-4}	4.6×10^{-4}
127	4.7×10^{-4}	1.3×10^{-4}	4.6×10^{-4}	3.8×10^{-4}	1.5×10^{-3}	9.0×10^{-4}
144	9.1×10^{-4}	6.9×10^{-4}		1.5×10^{-3}	2.4×10^{-3}	2.1×10^{-3}

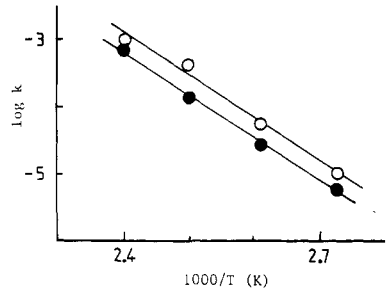

Figure 3. Plot of log k vs $1/T$ for Bu_4N^+-doped *cis*-PA (○) and *trans*-PA (●).

solution,[18] we postulate the following mechanism, which involves protonation of the carbanionic site by an α-hydrogen of the R_4N^+ ion. The destruction of doped sites along with the creation of sp^3 defects on the polymer accounts for the decrease of conductivity and spin mobility.

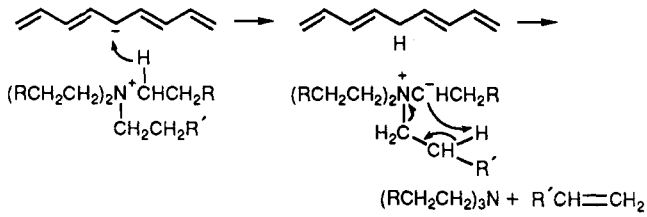

The ylide intermediate formed by the deprotonation of the R_4N^+ ion proceeds through an internal rearrangement to give more stable products, viz., a tertiary amine and an alkene. The observed first-order kinetics conforms to this mechanism. The above mechanism is further verified and confirmed by the characterization of the decomposed films and identification and quantitative evaluation of the byproducts as described below.

(1) IR Spectroscopy. A thin Bu_4N^+-doped *cis*-PA film was heated at 180 °C in a sealed tube for about 4 h. The resulting film was washed thoroughly with THF and dried. Comparison of the IR spectra of the pristine and the treated films shows a considerable increase of the absorptions in the region 3000 cm^{-1}, which confirms the formation of CH_2 groups by the heat treatment. The elemental analysis of the same film testifies the absence of any residual undecomposed Bu_4N^+ ions or Bu_3N, thereby excluding the possibility of attributing the CH_2 absorptions to the alkyl groups present in the latter.

(2) Elemental Analysis and Gas Chromatography. Elemental analysis of the degraded film coupled with GC analysis of the resultant products supplies quantitative evidence for the suggested mechanism. Two different PA films were separately doped with Bu_4N^+ and $Pent_4N^+$ (Pent = pentyl) ions. They were separately thermally degraded in sealed tubes at 180 °C for 4 h, and the degradation products were extracted with THF. The resulting films were subjected to elemental analysis. Bu_3N and Pen_3N were detected by GC. Using suitable

Table II
Activation Energies of the R_4N^+-Doped Samples and of Some Examples Reported in the Literature

polymer	counterion	activation energy, kcal/mol	ref
cis-PA	Bu_4N^+	29 ± 3	this work
trans-PA	Bu_4N^+	28 ± 3	this work
cis-PA	Oct_4N^+	28 ± 3	this work
trans-PA	Oct_4N^+	26 ± 3	this work
cis-PA	$Dodec_4N^+$	26 ± 3	this work
trans-PA	$Dodec_4N^+$	24 ± 3	this work
PA	iodine	16.1	3
PA	ClO_4^-	18.4	3
PA	$IrCl_6^{2-}$	17.9	3
PA	autooxidation	9.6	4
cis-PA	autooxidation	11.5	12
trans-PA	autooxidation	6.9	12
PA (modified)[a]	autooxidation	13.0	13
polypyrrole	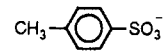	15.0	14
polypyrrole	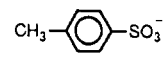	16.0	13

[a] Modified with chlorosulfonyl isocyanate.

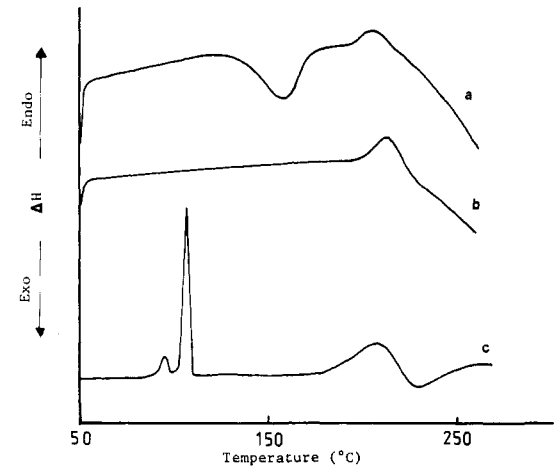

Figure 4. (a) DSC thermogram of Bu_4N^+-doped PA. (b) An identical sample annealed up to 200 °C, cooled, and scanned. (c) DSC thermogram of Bu_4NBr.

standard solutions, the amounts of the resulting tertiary amines were quantitatively determined. The molar ratio of H/C calculated from the elemental analysis of the degraded films and the Y calculated in terms of the tertiary amine produced are reported in Table IV. The Y values evaluated from the tertiary amine agree well with those determined by other methods such as weight increase, acidimetry, and elemental analysis, reported earlier.[7] This amply substantiates the proposed mechanism. The H/C ratios of the decomposed films are higher than expected from their reduction levels. This may be accounted for by considering a repeated elimination and redoping reaction taking place in the presence of the doping agent used

Table III
Thermal Characteristics of the DSC Thermograms of R_4N^+-Doped PA

counterion	isomer	onset of degrdatn, °C	max of exotherms, °C	degradatn completed, °C	ΔH, cal/g	E_A, kcal/mol	frequency factor
Bu_4N^+	cis	120	165	186	7.2	18 ± 2	2.5×10^8
$Dodec_4N^+$	cis	99	158	174	21	22 ± 2	1.6×10^{10}
$Dodec_4N^+$	trans	92	152	177	18	19 ± 2	3×10^9

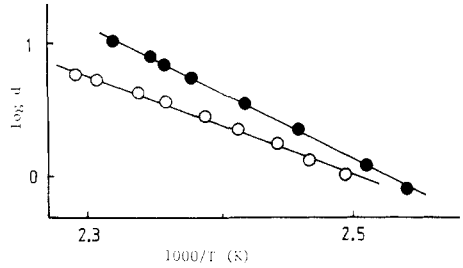

Figure 5. Plot of log d vs $1/T$, for the determination of activation energy from the DSC exotherms of (○) Bu_4N^+ and (●) $Dodec_4N^+$-doped *cis*-PA samples.

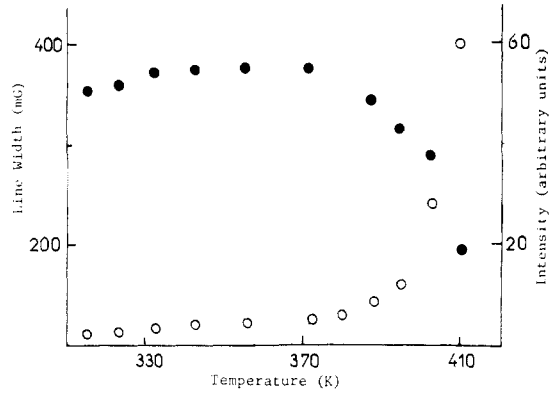

Figure 6. Variation of line width (○) and intensity (●) of ESR spectra of Bu_4N^+-doped *cis*-PA as a function of increasing temperature.

for their preparation, leading to accumulation of hydrogen atoms on the doped PA. We have already reported[7] that the maximum doping levels obtained in the case of R_4N^+ insertion, using benzophenone dianion as the reducing agent, are similar to those from benzophenone radical anion, even though the latter is a weaker electron donor.[19] The Y_{max} expected from the redox potential of benzophenone dianion is higher than 7%, but a limitation of the doping levels may arise from the instability of higher R_4N^+-doped samples.

In order to verify this point and due to the lack of complex carbanionic dopant systems of suitable redox potentials[7] that coud have helped in exceeding the 7–8% doping levels in the case of the R_4N^+ ions, we have resorted to an ion-exchange technique. It consists in the cation exchange between an alkali-metal-doped PA and the R_4NBr present in the solution, the reaction being driven forward by the very low solubility of the resulting alkali-metal bromide.

$$PA(Li^+) + Bu_4NBr \rightarrow PA(R_4N^+) + LiBr$$

Four different samples of PA were doped simultaneously with lithium naphthalenide in THF, washed, and dried by cryogenic pumping. One of the doped samples was deactivated with methanol vapors and dried; a second one was dedoped with fluorenone,[19] washed, and dried. Both of them were subjected to elemental analysis. The same H/C ratio as for pristine PA is found after dedoping with fluorenone (Table V); this excludes any protonation during doping. The increase of the H/C ratio after

Table IV
Elemental Analysis of the Degraded Film and GC Analysis of the Degradation Products

	H/C molar ratio		Y, %	
counterion	elem anal.	expected	GC anal.	expected[a]
Bu_4N^+	1.24	1.07	6.2	6.5
$Pent_4N^+$	1.27	1.07	6.0	6.5

[a] From ref 7.

Table V
Results of Ion-Exchange Technique

before exchange: dopant $NP^{\bullet-}Li^+$/THF		after exchange: Bu_4NBr/THF	
	H/C mole ratio from elem anal.		Y, %
pristine PA	1.03	wt uptake	9.9
doped film		acidimetry	8.2
*deactivated with methanol	1.15	amine detected by GC	4.8
*dedoped with fluorenone	1.02	H/C molar ratio of the film dedoped with fluorenone	1.09

deactivation with methanol is in good agreement with the doping level expected for $NpLi^+$ (Y = 15%).

The two other doped samples were immersed in THF containing pure and dry Bu_4NBr. When the exchange was complete the THF solution in which the exchange was carried out was cryogenically collected in another glass bulb in order to separate the tertiary amines that might have been formed during the exchange reaction from the Bu_4NBr in excess. The tertiary amine was quantitatively determined by GC analysis, and the absence of Bu_4NBr in the solution was confirmed by potentiometric titration for bromide. One of the two Bu_4N^+-doped samples prepared by exchange was dedoped with fluorenone and was subjected to elemental analysis. The other sample was washed, dried, and subsequently weighed in a drybox. A doping level of about 8–9% was determined from the weight uptake (assuming Bu_4N^+ as the effective counterion) and by direct titration of the methanolic solution originating from deactivation of the doped film. Inspection of Table V reveals that highly doped PAs are unstable in presence of R_4N^+ ions and they undergo deactivation by abstracting acidic protons from the latter. This reaction slows down as the basicity of the reduced PA reaches that corresponding to about 8% reduction. Within the limits of experimental error there is good concordance between the amine produced, the residual reduction level, and the excess hydrogen on the doped film.

The ion-exchange technique thus provides conclusive evidence for the conclusion that the limitation to attaining higher doping levels in the case of R_4N^+ ions is imposed by the reactivity of the reduced PA toward such counterions.

There is a close similarity between the reaction pathway discussed above, involving the reduced PA and its counterion (R_4N^+), and the one usually used to synthesize segmented PA.[20] The segmented PA is synthesized by the protonation of the carbanionic sites along the doped-

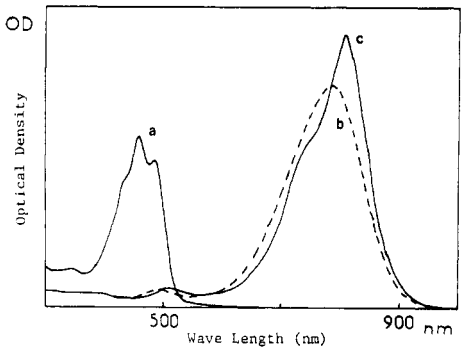

Figure 7. Optical spectra of β-carotene (a), that of its dianion associated with Na^+ (b), and that of its dianion associated with Bu_4N^+ (c) obtained by the ion exchange.

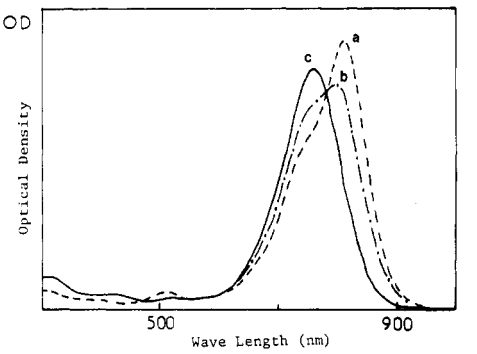

Figure 8. Optical changes during the transformation of β-carotene dianion associated with Bu_4N^+ to its protonated monoanion: (a) t = 0, (b) t = 1 h 30 min, (c) t = 5 h.

PA chain. The unexpected properties of the segmented PA thus formed were explained theoretically as due to an energetically favored clustering of the sp^3 defect sites.[21] It may then be asked to what extent this is true in the autodeactivation of the R_4N^+-doped PA. Although we have not examined this aspect in detail, such a possibility cannot be excluded.

(C) Model Study Using *trans*-β-Carotene. *trans*-β-Carotene (referred to as Car), a linear conjugated molecule containing 11 double bonds, serves as a suitable soluble model for PA. The β-carotene can be reduced chemically or electrochemically. A two-electron transfer to the β-carotene has been confirmed by chemical[10] and electrochemical methods,[22] thus ruling out the four-electron reduction suggested by Japanese authors.[23] The electrogeneration of the radical anion and the dianion occurs at −1.68 and −1.85 V (vs SCE), respectively. UV/visible spectroscopy is an efficient tool to study the reduction of β-carotene, due to the well-defined absorption maxima for β-carotene (458 nm) and its radical anion and dianion (848 and 790 nm, respectively, for Na^+ counterions).[10]

(1) R_4N^+ Salt of β-Carotene Dianion. The conventional method of reduction of β-carotene with an organoalkali-metal compound[10] produces the corresponding alkali-metal salt of the reduced β-carotene. Such a technique is inappropriate for the synthesis of R_4N^+ salt of β-carotene due to the instability of organo-R_4N^+ compounds having suitable redox potentials. We have therefore devised an indirect technique, which involves the synthesis of the sodium salt of the β-carotene dianion and its exchange with R_4N^+ ions.

$$\text{Car} + 2\text{Na} \rightarrow \text{Car}^{2-}(\text{Na}^+)_2$$

$$\text{Car}^{2-}(\text{Na}^+)_2 + 2\text{R}_4\text{NBr} \rightarrow \text{Car}^{2-}(\text{R}_4\text{N}^+)_2 + 2\text{NaBr}$$

The R_4N^+ salt of β-carotene dianion is instantaneously generated on adding R_4NBr to the dianion as can be realized from the anticipated bathochromic spectral shift from 790 nm toward 815 nm, accompanied by an increase of the molar absorption coefficient (see Figure 7). Figure 8 illustrates the transformation of this dianion into a species absorbing at 760 nm, for which an absorption coefficient of 2.7×10^5 L mol^{-1} cm^{-1} can be estimated. This transformation obeys a first-order kinetics with respect to the dianion, yielding a rate constant of 6.4×10^{-4} s^{-1}. The determination of rate constants in the temperature range 293–198 K furnishes an activation energy of 4.4 ± 0.5 kcal/mol.

Characterization of the product at 760 nm by ESR and UV/visible spectroscopy leads to the following conclusions. It is not a radical anion as it does not exhibit an ESR signal. It is incapable of effecting electron transfer

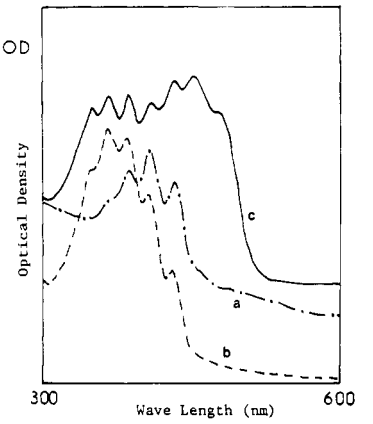

Figure 9. (a) Optical spectra of the product resulting from the spontaneous decomposition of the monoanion formed from the β-carotene dianion Bu_4N^+. (b) Optical spectra of the product resulting from the direct protonation of the monoanion formed from the β-carotene dianion Bu_4N^+. (c) Optical spectra of the product resulting from the direct protonation of the product formed from the β-carotene radical anion Bu_4N^+.

to β-carotene or to fluorenone, suggesting that the compound formed at 760 nm is a monocarbanion having a redox potential higher than those of the β-carotene radical anion (−1.68 V) or the fluorenone radical anion (−1.28 V). This monoanion is comparatively stable but slowly decomposes to yield protonated products whose absorption maxima are shifted further to shorter wavelengths (see Figure 9a). A comparison of this spectrum to that of the polyenes reported in the literature[24] enables the identification of the product as a 9-polyene. Similarly, the deactivation of this monocarbanion with methanol yields dihydrogenated β-carotenes whose spectral characteristics correspond (see Figure 9b) to a mixture of polyene sequences, viz., the 7 and 9 with a predominance of the 7. The same mixture of dihydrogenated β-carotenes can be generated by direct protonation of the β-carotene dianion.[10] All these observations can be accomodated by considering a noninstantaneous proton abstraction by the β-carotene dianion from one of its R_4N^+ counterions, producing a monoanion of β-carotene, which absorbs at 760 nm. The deprotonated R_4N^+ rearranges to stable products, viz., a tertiary amine and an alkene.

$$\text{Car}^{2-}(\text{R}_4\text{N}^+)_2 \rightarrow \text{HCar}^-(\text{R}_4\text{N})^+ + \text{NR}_3 + \text{alkene}$$

In order to clarify and confirm the feasibility of generating the monocarbanion by the partial hydrogenation of the β-carotene dianion by a proton donor, other than the R_4N^+ ion, we have made use of fluorene, which has a pK_a value very close to that of R_4N^+ ion, since the

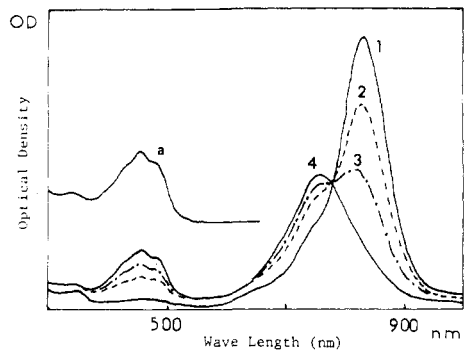

Figure 10. Optical spectral changes observed during the transformation of β-carotene radical anion Bu_4N^+ (Λ_{max} = 815) to β-carotene (Λ_{max} = 458) and β-carotene monoanion Bu_4N^+ (Λ_{max} = 760): (a) β-carotene, (1) t = 0, (2) t = 20 h, (3) t = 50 h, (4) t = 10 days.

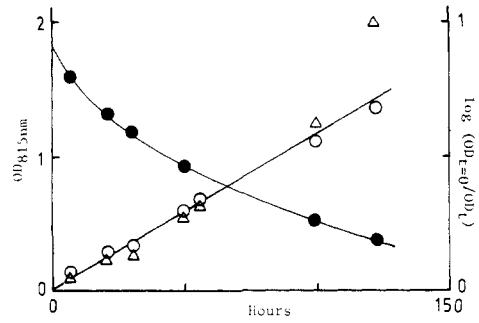

Figure 11. Kinetics of the transformation of the β-carotene radical anion to its monoanion and β-carotene: (○) first-order plot, (△) second-order plot.

conjugate base of the former was reported to be stable with the latter.[7]

As anticipated, fluorene brings about a controlled protonation of the dianion into a monoanion, absorbing at 760 nm, with simultaneous formation of the fluorenyl anion. This implies that the monoanion and the fluorenyl anion have comparatively similar basicities. A slow dihydrogenation also occurs to a certain extent. Therefore, we can conclude that the monoanion formed by the partial hydrogenation of the β-carotene dianion has a redox potential lower than that of the fluorenyl (−1.01 V vs SCE) and higher than that of the fluorenone radical anion (−1.28 V vs SCE). This is in accordance with the electrochemical studies on β-carotene reported by Mairanovsky et al.,[22] who observed the formation of such a monoanionic species, to which they assigned a redox potential of −1.19 V (vs SCE).

(2) R_4N^+ Salt of β-Carotene Radical Anion. A similar cation exchange leads to the R_4N^+ slat of the β-carotene radical anion but is not accompanied by the expected red shift, as is often the case with the carbanions and radical anions on being driven toward the free ion state due to the bulky countercation. The β-carotene radical anion associated with Na^+ ion absorbs at 848 nm whereas that with R_4N^+ ion absorbs at 810 nm. The intensity of the maximum fades slowly with the simultaneous appearance and growth of the peaks at 760 and 458 nm (Figure 10). The decreasing intensity of the peak at 810 nm, monitored as a function of time, fits a first-order decay kinetics, and a rate constant of 1.8×10^{-6} s^{-1} could be estimated (Figure 11).

The newly formed peak at 458 nm can be attributed to β-carotene whereas the one at 760 nm exhibits the same optical and ESR spectral characteristics as the one originating from the β-carotene dianion described in the previous section. When this solution, possessing absorption maxima at 458 and 760 nm, is deactivated directly with methanol (Figure 9c), the peaks corresponding to the β-carotene persist whereas the peak at 760 nm transforms to a mixture of shorter sequences of polyenes identical with that in Figure 9b. The slow proton abstraction by the β-carotene radical anion from the R_4N^+ ion to form the monoanion and β-carotene can be understood in light of similar protonation reactions of the classical radical anions described in the literature.

Two entirely different reaction pathways have been put forward. For example, the protonation of naphthalene radical anion in THF by ethanol has been suggested to proceed through the following steps.[25]

$$Np^{\bullet-} + BH \rightarrow NpH^{\bullet} + B^-$$

$$NpH^{\bullet} + Np^{\bullet-} \rightarrow NpH^- + Np$$

Since the formation of the protonated naphthalene radical is the rate-determining step, the reaction is first order with respect to the naphthalene radical anion.

On the other hand, the protonation of the perylene radical anion involves the presence of a disproportionation equilibria[26] and it is the perylene dianion that reacts with a proton donor to yield the monoanion.

$$2Py^{\bullet-} \rightleftharpoons Py^{2-} + Py$$

$$Py^{2-} + BH \rightarrow PyH^- + B$$

Here, the rate-limiting step involves the disproportionation equilibria. Consequently, the reaction is second order with respect to perylene radical anion.

In accordance with the above mechanisms, the protonation of β-carotene radical anion by the R_4N^+ produces equivalent amounts of the monohydrogenated anion and β-carotene. Due to the close proximity of the redox potentials of β-carotene dianion and its radical anion, the disproportionation equilibrium might be favored. Furthermore, the addition of a bulky cation like R_4N^+ is likely to shift the equilibrium to the right.[27]

$$2Car^{\bullet-} \rightleftharpoons Car^{2-} + Car$$

Hence, a second-order reactivity with respect to the radical anion is expected, but the precision of the experimental data presented in Figure 11 does not permit us to distinguish between first-order and second-order reactivity. Therefore, the extremely lower rate constant for the degradation of the β-carotene radical anion, compared to its dianion, might be due to either its higher redox potential (−1.68 vs SCE) or to its low disproportionation constant.

To sum things up, the reactivity of the reduced β-carotene toward its R_4N^+ countercation is not unexpected in view of the spontaneous decomposition of simple carbanionic salts of such R_4N^+ ions. It is possible to reconcile the order of their reactivities in terms of their respective redox potentials. From our previous investigation of the stability of such carbanionic systems, the only one to possess appreciable stability was found to be the fluorenyl R_4N^+ (−1.01 V vs SCE). All other systems having redox potentials lower than this limiting value are susceptible to a Hofmann type elimination reaction. Consequently, the polyconjugated reduced β-carotene does not claim to distinguish itself as nonreactive due to the greater charge delocalization.

Conclusion

Through a concerted evaluation of the instability of R_4N^+-doped PA by three different techniques and through

a parallel model study on reduced β-carotene containing R_4N^+ counterions, a reaction pathway for explaining the counterion-induced instability is established. Similar to that observed in the case of oxidized polypyrroles, where the aging characteristics were governed by their oxidation levels, the reactivities of the R_4N^+-doped PA are to a large extend regulated by their redox potentials. It appears that the PA possessing a reduction level of 7% (about −2 V vs SCE) should be more prone to protonation than the reduced β-carotene (−1.85 V vs SCE). On the contrary, the latter turns out to be more reactive than the former. This difference is explained by taking into account the unfavorable conformation in which the R_4N^+-complexed PA are confined due to their existence in the solid state. There is a similar difference between the activation energies of the processes taking place in the solid state or in the solution. The N-doped PA containing R_4N^+ counterions resemble the p-doped PA where the dopant anion interacts with the polymer backbone, leading to the deterioration of the properties. Nevertheless, in the case of R_4N^+-complexed PA, since the reactivities are governed by the redox potentials of the reduced PA, appreciable stability can be gained at the expense of the high reduction levels.

Acknowledgment. The authors are grateful to Maxime Bernard for the ESR and to Monique Scheer for the DSC measurements.

References and Notes

(1) Huq, R.; Farrington, G. C. *J. Electrochem. Soc.* **1984**, *131*(4), 819.
(2) Pochan, J. M. In *Handbook of Conducting Polymers*; Skotheim, T. A., Ed.; Dekker: New York, 1986; Vol. 2, p 1383.
(3) Druy, M. A.; Rubner, M. F.; Walsh, S. P. *Synth. Met.* **1986**, *13*, 207.
(4) Yang, X. Z.; Chien, J. C. W. *J. Polym. Sci., Polym. Chem. Ed.* **1985**, *23*, 859.
(5) Elsenbaumer, R. L.; Delnnoy, P.; Miller, G. G.; Forbes, C. E.; Murthy, N. S.; Eckhardt, H.; Baughmann, R. H. *Synth. Met.* **1985**, *11*, 251.
(6) Kaner, R. B.; Porter, S. J.; MacDiarmid, A. G. *J. Chem. Soc., Faraday Trans.* **1986**, *82*(1), 2323.
(7) Ignatious, F.; Francois, B.; Mathis, C. *Makromol. Chem.*, **1989**, *190*, 737.
(8) Ito, T.; Shirakawa, H.; Ikeda, S. *J. Polym. Sci., Polym. Chem. Ed.* **1974**, *12*, 11.
(9) Ignatious, F.; Francois, B.; Mathis, C., *Synth. Met.* **1989**, *32* (3), 283.
(10) Rudatsikira, A.; Francois, B.; Mathis, C. *Makromol. Chem.* **1989**, *190*, 93.
(11) Mathis, C.; Francois, B. *Synth. Met.* **1984**, *9*, 347.
(12) Rolland, M.; Bernier, P.; Aldissi, M. *Phys. Status Solidi A* **1980**, *62*, K5.
(13) Munstedt, H. *Polymer* **1988**, *29*, 296.
(14) Samuelson, L. A.; Druy, M. A. *Macromolecules* **1986**, *19*, 824.
(15) Ito, T.; Shirakawa, H.; Ikeda, S. *J. Polym. Sci., Polym. Chem. Ed.* **1975**, *13*, 1943.
(16) Rogers, R. N.; Morris, E. D. Jr. *Anal. Chem.* **1966**, *38*(3), 412. Rogers, R. N.; Smith, L. C. *Anal. Chem.* **1967**, *39*(8), 1024.
(17) Rachdi, F.; Bernier, P. *Mol. Cryst. Liq. Cryst.* **1985**, *117*, 121. Bernier, P.; El-Khodary, A.; Rachdi, F.; Fite, C. *Synth. Met.* **1987**, *17*, 413.
(18) March, J. *Advanced Organic Chemistry*, 3rd ed.; Wiley: New York, 1985; p 908.
(19) Francois, B.; Mathis, C. *Synth. Met.* **1986**, *16*, 105.
(20) Yang, X. O.; Tanner, D. B.; Arbuckle, G.; MacDiarmid, A. G.; Epstein, A. J. *Synth. Met.* **1987**, *17*, 277.
(21) Clough, S.; Tripathy, S.; Sun, X. F.; Orchard, B.; Wnek, G. *Makromol. Chem., Rapid Commun.* **1988**, *9*, 535.
(22) Mairanovsky, V. G.; Engovatov, A. A.; Ioffee, N. T.; Samokuvalov, G. I. *J. Electroanal. Chem.* **1975**, *66*, 123.
(23) Takahashi, R.; Tachji, I. *Agric. Biol. Chem.* **1962**, *26*, 771. Yasuyoshi, J. T.; Saito, Y.; Shimizu, M.; Tanaka, C.; Tanaka, M.; *Bull. Chem. Soc. Jpn.* **1987**, *60*, 1595.
(24) Daniels, V. D.; Reeb, N. H. *J. Polym. Sci., Polym. Chem. Ed.* **1974**, *12*, 2115.
(25) Paul, D. E.; Lipkin, P.; Weissmann, S. I. *J. Am. Chem. Soc.* **1956**, *78*, 116.
(26) Levin, G.; Stephen, C.; Szwarc, M. *J. Am. Chem. Soc.* **1972**, *94*, 2652.
(27) Zabolotny, E. R.; Garst, J. F. *J. Am. Chem. Soc.* **1964**, *86*, 1645. Smentowski, F. J.; Stevenson, G. R. *J. Phys. Chem.* **1969**, *73*, 340.